

# The variability and radial velocity of planetary nebulae central stars.

Ali, A.<sup>1\*</sup>, Mindil, A.<sup>2</sup>

<sup>1</sup> Astronomy, Space Science & Meteorology Department, Faculty of Science, Cairo University, Giza 12613, Egypt.; *afouad@sci.cu.edu.eg*

<sup>2</sup> Department of Physics, College of Science, University of Jeddah, Jeddah, Saudi Arabia.; *amindil@uj.edu.sa*

Received 20XX Month Day; accepted 20XX Month Day

## Abstract

The extremely accurate estimates of stellar variability and radial velocity in the Gaia Data Release 3 (Gaia DR3) have enabled us to examine the close binarity and radial velocity (RV) of central stars (CSs) of planetary nebulae (PNe). This study is twofold: (1) searching for new close binary CSs candidates to better understand how binarity affects the formation and evolution of PNe; and (2) extending the sample size of known RV of PNe in order to understand their kinematics and the dynamics of the Milky Way. As a target sample, we used all true, possible, and likely PNe available in the literature. Then, we looked for their matched Gaia DR3 sources that provide measurements of variability and RV. As a result, we detected the first large collection of trustworthy photometric variability of 26 symbiotic stars (SySts) and 82 CSs. In this CS group, there are 24 sources already classified as true close binary CSs in the literature. Hence, we discovered 58 new close binary CS candidates. This close binary (CB) sample represents more than half of what is currently available in the literature. In addition, we identified the radial velocities for 51 PNe. To our knowledge, 24 of these were measured for the first time. The RV measurements predicted by Gaia, based on the Doppler shift of the CS absorption lines, and those derived from nebular emission lines, show satisfactory agreement except for a few extremely high-velocity PNe.

---

\* Corresponding author

**Key words:** Planetary nebulae: stellar variability - radial velocity

## 1 INTRODUCTION

Gaia is an ESA project that aims to create a 3-D representation of the Milky Way galaxy. The Gaia Data Release 1 (Gaia DR1) appeared in September 2016. This was followed by Gaia Data Release 2 (Gaia DR2) in April 2018 and Early Data Release 3 (Gaia EDR3) in December 2020. The Gaia DR3 was published on June 13, 2022. It provides positions and apparent magnitudes of  $\sim 1.8$  billion sources, as well as parallaxes, proper motions, and colors of  $\sim 1.5$  billion objects. In comparison to Gaia DR2, Gaia DR3 exhibits significant improvements in astrometric and photometric accuracy, precision, and homogeneity. In addition to updating earlier releases, Gaia EDR3 contains new data, such as astrophysical parameters (Creevey et al. 2022), BP/RP spectra (De Angeli et al. 2022), and variability classification (Eyer et al. 2022). According to Eyer et al. (2022), Gaia DR1 has  $\sim 3000$ , Gaia DR2 has  $\sim 550,000$ , and Gaia DR3 has  $\sim 10.5$  million variable sources.

The topic of binarity has important implications for our understanding of cataclysmic variables and novae, type Ia supernovae, symbiotic stars, and other phenomena such as the production of astrophysical jets (Boffin & Jones 2019). Binary interactions occur between stars of all sizes and orbital separations, ranging from compact white dwarfs with 5-minute orbital periods to giant stars with hundred-year orbital periods. From an observational and theoretical perspective, all stars with masses ranging from 1 to 8 solar masses—roughly 95% of the galaxy’s stellar population—will undergo the PN stage of evolution. As a consequence, studying the binary CSs of PNe is crucial to our understanding of many astrophysical phenomena that have traditionally been attributed to single-star evolution (Aller et al. 2020).

The HASH catalog (Parker et al. 2016) contains  $\sim 3500$  PNe, with 80% displaying complex morphologies that differ from sphericity, such as elliptical, bipolar, and multipolar PNe, as well as various internal features such as multi-shells, jets, and knots. Currently, there is widespread agreement on the importance of CS binarity in understanding PNe divergence from sphericity, where the various morphologies of PNe can no longer be explained by single-star models. Since the number of detected binary CSs has increased significantly over the past decade, it has become obvious that the wide variety of PNe morphologies and some of their unusual chemical properties are the products of binary evolution. A common-envelope event is the best method for generating an axisymmetric PN via binary interaction. The CB fraction is the most rigorous binarity test in PN formation. Despite the challenge of finding CS infrared excesses, De Marco et al. (2013) successfully employed the technique to calculate a binary fraction, obtaining a value of 67–78% based on I-band excess and 100–107% based on J-band excess.

Douchin et al. (2015) obtained I-band fraction of  $40\pm 20\%$  and J-band fraction of  $62\pm 30\%$  using an improved method and a larger sample. Estimates of the binary fraction range from 20% for photometrically detectable CB to 60-80% for those identified using the radial velocity variability and infrared excesses approaches. According to Boffin & Jones (2019), the bipolar and multipolar PNe are the result of CB stellar evolution. Wesson et al. (2018) identified a link between the high abundance discrepancy factors (adfs) of PNe and their CSs binarity. It was found that all PNe of binary CSs with a period less than 1.15 days had adfs larger than 10 and electron densities of less than  $1000\text{ cm}^{-3}$ , whereas those with longer periods had lower adfs and significantly higher electron densities. In addition, they noted that any PN with an extreme adf must contain a close binary CS.

In addition to ground-based observations of close binary CSs (e.g. Hillwig et al. (2016), Miszalski et al. (2011b), Jones et al. (2010), Miszalski et al. (2009)), space-based observations, such as those from the Transiting Exoplanet Survey Spacecraft-TESS (Aller et al. 2020) and Kepler satellite (Jacoby et al. 2021), have detected a significant number of CB candidates. Most of the photometric variability of these objects can be attributed to the effect of a companion star on the nebular CS.

Gaia DR3 has radial velocities for  $\sim 34$  million stars and RV spectrometer spectra for almost a million stars (Katz et al. 2022). The Gaia Data Release 4 (Gaia DR4), which will analyze 66 months of data, will extend all RV spectra to a G-magnitude of 16.2 and reveal the RV of  $\sim 100$  million stars.

In the present article, we aim to uncover the variability and RV of the CSs of PNe using the recent release of the Gaia project. We showed the PNe data sample and the approach used for extracting the variability and RV from the Gaia DR3 database in Section 2. Section 3 contains the results and discussion, whereas Section 4 has the conclusions.

## 2 THE VARIABILITY AND RV DATA.

The RV spectrometer is a medium-resolution spectrograph ( $R \approx 11500$ ) covering the wavelength range 846 – 870 nm (Cropper et al. 2018). In total,  $\sim 10.5$  million objects have been identified as variables in the Gaia DR3. Eyer et al. (2022) have reported the presence of 35 types and sub-types of variable objects, where the output of the variability analysis amounts to 17 tables containing a total of 365 parameters. The stellar photometric variability is stored in the `gaiadr3.gaia_source` table in the field `phot_variable_flag`. The combined RVs and their formal uncertainties are, respectively, stored in the `radial_velocity` and `radial_velocity_error` fields in the `gaiadr3.gaia_source` table.

To achieve the goals of this article, we searched the Gaia DR3 database for all stars whose positions matched those of PN central stars listed in the HASH catalog as true, possible, and likely PNe.



### 3.2 Radial velocity of PNCSSs

The pioneering work for determining the RV of PNe was given by Schneider & Terzian (1983) who published the heliocentric RV for 524 PNe. The next compilation (867 PNe) was reported by Durand et al. (1998). Beaulieu et al. (1999) reported the RV of 45 PNe lying in the southern galactic bulge. Based on high dispersion spectra, Richer et al. (2017) reported the RV of 76 PNe. Numerous other individual RVs are scattered throughout the literature (e.g. Ali et al. 2016; Ali & Dopita 2017, 2019). All the above measurements were derived from the Doppler shift of the nebular spectra. The Gaia mission opened a new window for calculating the RV from the spectra of the observed CSs. The Gaia RV was found by measuring the Doppler shift of a template spectrum and then comparing it to the spectrum that was seen.

Using the current release, we were able to detect the RV for 51 PNe, including updated values for 14 PNe recorded by Ali et al. (2022). Table 3 lists the newly detected radial velocities by Gaia DR3 and those obtained by Durand et al. (1998). The estimated median uncertainty of this compilation is 12.2%. In Figure 1, we compared the new RV measurements with those given by Durand et al. (1998). The diagonal line indicates the 1:1 matches. In general, the RVs computed from the spectra of both the CSs (Gaia DR3) and their associated nebulae are in good agreement. However, there are a few outliers related to high-velocity objects, such as H 2-24, SB 15, and Th 3-14. At first glance, all outlier objects have galactic longitudes of 0 to 10 and 350 to 360 degrees, and galactic latitudes of 0 to  $\pm 10$  degrees, indicating that they are located in the direction of the galactic bulge. To figure out the cause of this discrepancy, we examined the possible physical reasons, such as the interaction between planetary nebulae and the interstellar medium (ISM), the effect of nebular electron density, and the accuracy of radial velocity measurements deduced from PNe and CSs. We found that none of these nebulae interact with the ISM, and the available electron density data for these objects did not provide a reasonable explanation. In addition, the accuracy of RV measurements derived from nebular emission lines is suitable. Thus, we examined the parameters that Gaia used to calculate the RV. We extracted two additional parameters relevant to the Gaia RV calculations: `rv_nb_transits` (the number of transits used to calculate the RV) and `rv_visibility_periods_used` (the number of visibility periods used to estimate the RV). Table 3, shows the previous two parameter values in columns 6 and 7. The preceding two parameters show that these outliers have a lower number of transits and shorter visibility periods compared with other RV measurements in Table 3. As a result, we may infer that the difference in RV measurements between the Gaia and nebular lines for these outlier objects is due to Gaia's inaccurate RV measurements.

## 4 CONCLUSIONS

We have discovered 82 planetary nebulae associated with close binary central star candidates. To our knowledge, 58 members of this group have been found for the first time. This group of close binary central stars comprises roughly half of all objects known in the literature. We also discovered photometric variability in 26 symbiotic stars and four stars of different types. Moreover, we detected the radial velocities of 51 planetary nebulae, 27 of which were identified for the first time. With a few exceptions, there is good agreement between the radial velocities measured from the absorption lines of the central stars and those measured from the emission lines of the planetary nebulae. In future work, we plan to extract the available photometric variability identifiers from the Gaia DR3 database to build the light curves for some of the objects mentioned in Table 1. We also plan to use the 74-inch telescope at the Kottami observatory, Egypt, to perform a time-series photometric study for a few of the detected close binary central star candidates. Simultaneously, we will search the TESS and Kepler Sky Surveys, as well as the OGLE variable star catalog, for data that will allow us to confirm the binarity of the newly detected objects.

**Acknowledgements** The authors would like to thank the reviewer for his or her constructive suggestions that helped enhance the original manuscript.

## References

- Afşar, M., & Ibanoglu, C. 2008, MNRAS, 391, 802
- Ali, A., Algarni, E., Mindil, A., & Alghamdi, S. A. 2022, Research in Astronomy and Astrophysics, 22, 085013
- Ali, A., & Dopita, M. A. 2017, PASA, 34, e036
- Ali, A., & Dopita, M. A. 2019, MNRAS, 484, 3251
- Ali, A., Dopita, M. A., Basurah, H. M., et al. 2016, MNRAS, 462, 1393
- Aller, A., Lillo-Box, J., Jones, D., Miranda, L. F., & Barceló Forteza, S. 2020, A&A, 635, A128
- Beaulieu, S. F., Dopita, M. A., & Freeman, K. C. 1999, ApJ, 515, 610
- Boffin, H. M. J., & Jones, D. 2019, The Importance of Binaries in the Formation and Evolution of Planetary Nebulae
- Chornay, N., Walton, N. A., Jones, D., et al. 2021, A&A, 648, A95
- Ciardullo, R., Bond, H. E., Sipior, M. S., et al. 1999, AJ, 118, 488
- Corradi, R. L. M., García-Rojas, J., Jones, D., & Rodríguez-Gil, P. 2015, ApJ, 803, 99
- Creevey, O. L., Sordo, R., Pailler, F., et al. 2022, arXiv e-prints, arXiv:2206.05864
- Cropper, M., Katz, D., Sartoretti, P., et al. 2018, A&A, 616, A5

- De Angeli, F., Weiler, M., Montegriffo, P., et al. 2022, arXiv e-prints, arXiv:2206.06143
- De Marco, O., Passy, J.-C., Frew, D. J., Moe, M., & Jacoby, G. H. 2013, MNRAS, 428, 2118
- Douchin, D., De Marco, O., Frew, D. J., et al. 2015, MNRAS, 448, 3132
- Durand, S., Acker, A., & Zijlstra, A. 1998, A&AS, 132, 13
- Exter, K. M., Pollacco, D. L., & Bell, S. A. 2003, MNRAS, 341, 1349
- Eyer, L., Audard, M., Holl, B., et al. 2022, arXiv e-prints, arXiv:2206.06416
- Hillwig, T. C., Bond, H. E., Frew, D. J., Schaub, S. C., & Bodman, E. H. L. 2016, AJ, 152, 34
- Hkiewicz, K., & Mikołajewska, J. 2017, A&A, 606, A110
- Jacoby, G. H., Hillwig, T. C., Jones, D., et al. 2021, MNRAS, 506, 5223
- Jones, D., Lloyd, M., Santander-García, M., et al. 2010, MNRAS, 408, 2312
- Katz, D., Sartoretti, P., Guerrier, A., et al. 2022, arXiv e-prints, arXiv:2206.05902
- Miszalski, B., Acker, A., Moffat, A. F. J., Parker, Q. A., & Udalski, A. 2009, A&A, 496, 813
- Miszalski, B., Corradi, R. L. M., Boffin, H. M. J., et al. 2011a, MNRAS, 413, 1264
- Miszalski, B., Jones, D., Rodríguez-Gil, P., et al. 2011b, A&A, 531, A158
- Munday, J., Jones, D., García-Rojas, J., et al. 2020, MNRAS, 498, 6005
- Parker, Q. A., Bojičić, I. S., & Frew, D. J. 2016, in Journal of Physics Conference Series, Vol. 728, Journal of Physics Conference Series, 032008
- Pollacco, D. L., & Bell, S. A. 1994, MNRAS, 267, 452
- Richer, M. G., Suárez, G., López, J. A., & García Díaz, M. T. 2017, AJ, 153, 140
- Schneider, S. E., & Terzian, Y. 1983, ApJ, 274, L61
- Wesson, R., Jones, D., García-Rojas, J., Boffin, H. M. J., & Corradi, R. L. M. 2018, MNRAS, 480, 4589

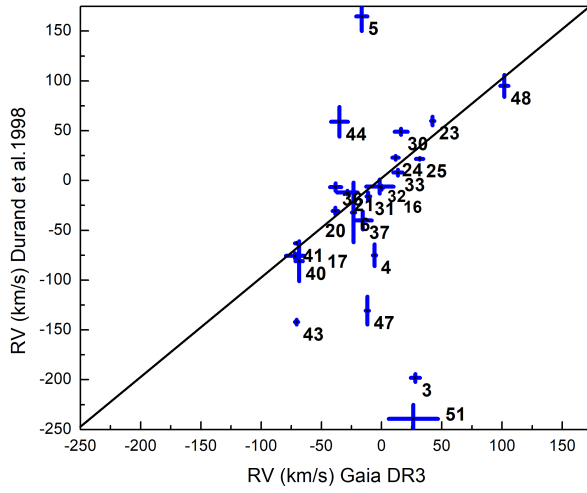


Fig. 1: The RVs derived from the Gaia DR3 against those reported by Durand et al. (1998). The diagonal line refers to the 1:1 correlation. The numbers on the plot assign the PNe numbers that listed in Table 3.

Table 1: The variable CSs in Gaia DR3. The magnitude and color of the CS are indicated by the G and B-R parameters, respectively. The letters T, L, and P stand for true, likely, and possible PNe. Bipolar, elliptical, round, irregular, and quasi-Stellar PN shapes are denoted by the primary morphological keys B, E, R, I, and S, respectively. Multiple shells, point symmetry, ring structure, and asymmetry are denoted by the internal structure symbols m, p, r, and s, respectively.

PN Name	l	b	Gaia DR3 designation	G	B-R	PN Status	Shape	Ref.	PN Name	l	b	Gaia DR3 designation	G	B-R	PN Status	Shape	Ref.
PN PC 12	0.17	17.25	4130784921205604736	15.2	0.6	T	Bmpr	1	IC 2165	221.32	-12.39	2999839084924027776	17.5	-0.2	T	Emrs	
PN BI O	0.88	-1.57	4056603178196321792	16.5	1.8	T	S		PPP 1	222.13	3.91	3058094200264637312	15.8	-0.6	T	Rar	
PPA J1800-2904	1.52	-2.85	4062356711999251328	18.1		T	s		PN M 3-2	240.37	-7.63	5609860130542365824	16.3	0.5	T	Bms	
PN ShW 7	1.80	-3.88	4050366645122261504	17.9	1.2	T	B	2	PG 1034+001	247.55	47.75	3806885288337214848	13.2	-0.6	T	na	11
Terz N 2111	3.96	1.66	4067312696253910272	16.9	4.4	T	Ea		PN K 1-2	253.58	10.78	5647809392112960000	17.0	0.2	T	Baps	12
PN H 2-24	4.33	1.84	4068460105422978048	15.3	4.3	T	Ba		PN M 3-6	253.97	5.78	5639472001599302528	13.2	0.0	T	E	
PN HF 2-2	5.14	-8.90	404849702430900064	17.2	0.0	T	Ems	3	LoTr 3	265.11	-4.21	5521499734013833984	13.0	0.7	T	Rr	
PN H 2-22	6.34	3.33	4117062676912301184	18.5	1.6	T	B		PN Lo 4	274.31	9.11	5414927915911816704	16.6	-0.4	T	Ears	
PN PBOZ 29	6.59	3.41	4118615354715439872	16.1	1.6	L	S		Wray 16-55	277.62	-1.73	5308685822467307008	12.2	5.9	T	S	
NGC 6629	9.41	-5.05	4089517157442187008	12.7	0.5	T	Ems		PN G281.1-00.4	281.18	-0.48	5259854002824501248	17.7	3.3	P	na	
PN A66 41	9.66	10.51	4136835641106850432	16.2	0.3	T	Ba	4	PN K 1-22	283.67	25.31	5399388964749811456	16.7	0.4	T	Ears	13
PN Sa 3-111	14.27	4.21	4147061232357104384	17.0	3.7	T	S		DS 1	283.90	9.73	5362804330246457344	12.1	-0.3	T	Imss	2
PN M 1-46	16.45	-1.98	4103910524954236928	12.8	0.8	T	Rmprrs		<b>Hen 2-70</b>	293.61	1.20	5335879596943573888	15.7	2.0	T	Bumps	
PTB 43	16.62	-4.05	410282536944868480	17.3	0.9	T	S		NGC 4361	294.11	43.63	3519614068578061568	13.1	-0.5	T	Emps	
PN PM 1-308	34.58	-11.75	4210278482327706496	13.1	0.6	T	na		PN G305.9-01.2	305.93	-1.27	5859151160662602752	19.3	2.9	T	B	
<b>PN G039.0-04.0</b>	39.08	-4.10	4292267621344388864	14.3	1.5	T	Emr		Hen 2-99	309.00	-4.24	5851865148069389568	13.2	0.4	T	Ers	
VSP 2-30	49.32	2.38	4320639728629291776	13.6	1.2	L	S		PN SuWi 2	311.05	2.48	5870592987893097984	11.9	0.6	T	Eamrs	
PN A66 63	53.89	-3.03	1820963913284517504	15.0	0.3	T	Bps	5,6,7	Hen 2-107	312.61	-1.90	5854138766383247232	14.6	1.2	T	Ea	
NGC 6891	54.20	-12.11	1803234906762692736	12.3	-0.2	T	Emrs	8		329.08	1.96	5982072132545824128	13.7	0.7	T	Ramrs	3,4
PN G054.5+01.8	54.59	1.85	4515887189511585792	18.6	1.4	L	E		<b>PN Mz 3</b>	331.73	-1.01	5934701559547878144	13.2	1.8	P	na	
PN A66 46	55.41	16.03	458538181764302528	15.0	-0.2	T	Eas	5,6,7	PN HaTr 7	332.51	-16.91	5911656865276078080	14.8	-0.3	T	Eas	3
PN K 3-51	56.83	-6.96	1821791540606971152	17.2	-0.1	T	R		IC 4642	334.39	-9.35	592334773032038528	15.9	-0.2	T	Ems	
IRAS 19461+2419	60.99	-0.57	2020643612977496704	18.6	2.5	T	S		PN HaTr 4	335.25	-3.62	5937103069115240192	16.8	0.7	T	B	
NGC 6720	63.17	13.98	2090486618786534784	15.6	-0.5	T	Emrs		MPA J1637-4911	335.95	-1.35	5940883018248096640	17.2	2.2	L	S	
PN Ps 1	65.02	-27.31	1745948362385436544	14.7	0.3	T	s		Hen 2-248	341.51	-9.18	594683168537720576	15.4	-0.3	T	S	2
ETHOS 1	68.10	10.99	2050526964622031744	17.2	-0.1	T	Bmps	9,10	NGC 6026	341.60	13.70	6011169161583903488	13.1	0.1	T	Eas	2
MWP 1	80.36	-10.41	1855295171732158080	13.0	-0.5	T	Baps		IC 1266	345.24	-8.83	5954912374289120896	11.3	0.0	T	Rars	
PN M 1-77	89.38	-2.27	1971995510535755648	11.9	1.0	T	Sm		PN Te1	345.24	-8.83	5954912374289120896	11.3	0.0	T	Rars	
PN K 1-16	94.03	27.43	2160562927224840576	15.0	-0.6	T	B		IC 4637	345.48	0.14	5966769881320062208	12.5	0.6	T	Eaprs	
NGC 40	120.02	9.87	537481007814722688	11.5	0.3	T	Bms		PPA J1747-3435	355.33	-3.21	4041711044735017856	18.8	0.8	T	Es	2
PB 9	122.72	70.36	1531053247144552704	18.0	0.7	T	Eams		PN M 1-27	356.53	-2.39	4053955824662571648	13.9	1.4	T	R	
PB 4	123.11	70.19	1531068915184317568	17.3	0.6	T	Emrs		PN M 4-4	357.03	2.44	4058620300979161660	16.5	3.8	T	Ear	1
PB 1	123.18	70.08	1531072827896228352	17.9	0.3	T	Ems		PN Al 2-O	358.01	-2.74	4043622756199128064	16.0	2.4	T	E	2
NAME TS 01	136.00	55.97	846615127231002880	18.0	-0.3	T	Es		PN Al 2-R	358.75	-2.76	4055678213978728320	15.4	5.3	T	B	
PN HFG 1	136.38	5.55	468033345145186816	14.0	0.7	T	Eamrs	2	PHR J1752-3116	358.77	-2.50	4055698280071328640	16.1	3.4	T	S	
<b>NGC 1501</b>	144.56	6.55	473712872456844544	14.2	0.6	T	Ems		JaSt 65	358.99	-1.55	4055974360527366272	17.7	2.4	T	S	
LTNF 1	144.81	65.85	786919754746647424	15.1	0.4	T	Bas	2	PN M 3-16	359.18	-2.30	4056131006637615488	17.1	1.1	T	Em	2
NGC 2371	189.16	19.84	885587110718845568	14.8	-0.4	T	Bmps		PN PM 1-166	359.24	1.22	4060159376692627840	15.3	3.2	P	B	
PN MaC 2-1	205.87	-26.73	3211200438511961088	15.8	-0.4	T	S		PN M 3-44	359.39	-1.81	4056355822397882880	16.0	2.1	T	B	
PN A66 30	208.56	33.29	660071056749861888	14.4	-0.2	T	Ramrs	1	PN Th 3-35	359.39	1.40	4060214180437611904	19.8	2.8	T	S	1
PHR J0650+0013	212.64	-0.07	3113542949606809088	15.2	1.1	T	Bmps		Terz N 19	359.89	5.25	4109665712365779968	19.0	1.1	T	B	

(1) Jacoby et al. (2021); (2) Miszalzi et al. (2009); (3) Hillwig et al. (2016); (4) Jones et al. (2010); (5) Pollacco & Bell (1994); (6) Afşar & İbanoğlu (2008); (7) Corradi et al. (2015); (8) Douchin et al. (2015); (9) Miszalzi et al. (2011a); (10) Munday et al. (2020); (11) Aller et al. (2020); (12) Exter et al. (2003); (13) Ciardullo et al. (1999).

Table 2: The variable symbiotic stars in Gaia DR3.

#	target_id	l	b	Gaia DR3 designation	G	B-R	Type
1	PN ShWi 5	1.21	-3.90	Gaia DR3 4050209822908746240	15.3	1.2	Symbiotic Star
2	PN H 1-45	2.02	-2.06	Gaia DR3 4062646712567004416	14.3	3.0	Symbiotic Star
3	PN Ap 1-11	3.12	-4.63	Gaia DR3 4050848540419995776	13.2	3.1	Symbiotic Star
4	PN H 2-43	3.49	-4.87	Gaia DR3 4050670827750135040	13.6	1.2	Symbiotic Star
5	IRAS 17554-2628	3.58	-1.22	Gaia DR3 4064034330564300928	19.8	2.8	Symbiotic Star
6	PN M 3-18	7.57	1.44	Gaia DR3 4070389125449668608	11.9	5.0	Symbiotic Star
7	PN Th 4-4	8.31	3.73	Gaia DR3 4119029875002043392	14.6	3.4	Symbiotic Star
8	PN M 2-9	10.90	18.06	Gaia DR3 4335188603873318656	13.9	1.3	Symbiotic Star
9	PN K 3-9	23.91	-1.54	Gaia DR3 4155672680486693120	15.3	2.6	Symbiotic Star
10	PN Ap 3-1	37.64	-2.97	Gaia DR3 4268140453591785984	14.3	3.9	Symbiotic Star
11	PN M 4-16	61.79	2.11	Gaia DR3 2022052808961769088	16.6	1.3	Symbiotic Star
12	Hen 2-468	75.94	-4.44	Gaia DR3 1870194997404105856	12.6	2.8	Symbiotic Star
13	PN M 1-2	133.12	-8.64	Gaia DR3 360112911622101120	12.6	1.2	Symbiotic Star
14	Hen 2-34	274.19	2.58	Gaia DR3 5409069172514684416	14.7	2.7	Symbiotic Star
15	Hen 2-25	275.22	-3.71	Gaia DR3 5310613021532357632	14.7	0.8	Symbiotic Star
16	Hen 2-106	312.03	-2.03	Gaia DR3 5853777267581362176	13.3	0.8	Symbiotic Star
17	Hen 2-104	315.48	9.46	Gaia DR3 6089564718596906880	13.6	0.8	Symbiotic Star
18	Hen 2-134	319.22	-9.35	Gaia DR3 5822400362454690688	12.1	2.5	Symbiotic Star
19	Hen 2-127	325.54	4.18	Gaia DR3 5889726659221998592	14.5	2.4	Symbiotic Star
20	PN Cn 1-2	326.41	-10.94	Gaia DR3 5818044445302448000	10.6	1.8	Symbiotic Star
21	PN Cn 1-1	330.78	4.15	Gaia DR3 5982979264021123968	10.8	1.1	Symbiotic Star
22	Hen 2-156	338.94	5.36	Gaia DR3 5992529686406981248	12.4	2.1	Symbiotic Star
23	Hen 2-176	339.39	0.74	Gaia DR3 5943382139466094720	13.6	4.1	Symbiotic Star
24	Hen 2-171	346.03	8.55	Gaia DR3 6020686328090453888	14.9	5.5	Symbiotic Star
25	PN H 2-4	352.95	3.93	Gaia DR3 5979902864926562176	14.2	3.2	Symbiotic Star
26	PN M 2-24	356.99	-5.80	Gaia DR3 4042147516455759744	15.1	0.8	Symbiotic Star
27	PN Th 3-20	357.41	2.62	Gaia DR3 4058701527427641472	14.0	2.8	Symbiotic Star
28	PN K 4-26	37.18	-6.85	Gaia DR3 4263728319553777408	13.9	6.7	Mira Variable Candidate
29	PN K 4-36	44.44	-10.38	Gaia DR3 4290522180961855872	12.7	4.7	M star
30	CD-48 6027	283.90	9.73	Gaia DR3 5362804330246457344	12.1	-0.3	Hot Subdwarf
31	Hen 2-58	289.18	-0.70	Gaia DR3 5338220285385672064	7.3	0.9	Wolf-Rayet

Table 3: The CS radial velocity of PNe in Gaia DR3. The symbol (:) in column 4 refers to the RV measurement with high uncertainty.

#	PN name	Galactic coordinate		RV (km/s)		rv_nb_transits	rv_visibility_periods_used
		l	b	Gaia DR3	Durand et al. (1998)		
1	MPA J1803-3043	0.4	-4.22		-130.5±6.0	3	2
2	Ap 1-11	3.12	-4.63	62.0±3.9		4	4
3	H 2-24	4.33	1.84	28.0±3.8	-198.2± 4.1	6	3
4	M 1-44	4.97	-4.96	-5.9±0.5	-75±11	4	4
5	SB 15	9.3	-6.53	-16.5 ± 4.7	165 ± 15	5	4
6	PN G009.8-07.5	9.87	-7.56	-23.3 ± 1.1	-32 ± 30	2	2
7	PN V-V 3-4	13.45	-4.25	-16.3 ± 4.7		7	7
8	UCAC4 374-117003	15.54	0.34	21.3 ± 2.2		8	8
9	SS 318	17.02	11.1	-36.7 ± 2.4		19	11
10	K 2-7	19.41	-19.66	-18.4 ± 0.5		14	12
11	PN G019.5-04.9	19.53	-4.96	-20.9 ± 1.4		13	9
12	Pe 1-15	25.91	-2.18	37.7 ± 3.7		6	4
13	IPHASX J191716.4+033447	39.08	-4.1	-4.2 ± 8.6:		9	9
14	K 1-14	45.61	24.32	-19.0 ± 1.0		63	22
15	VSP 2-30	49.32	2.38	-13.4 ± 1.9		27	18
16	Me 1-1	52.54	-2.96	-1.5 ± 11.4:	-6 ± 7	10	8
17	NGC 7008	93.41	5.49	-71.9 ± 7.7	-75.7 ± 2.7	18	11
18	IRAS 21282+5050	93.99	-0.12	28.2 ± 7.3		20	15
19	K 1-6	107.04	21.38	-55.7 ± 13.7		13	13
20	A 82	114.07	-4.67	-38.4 ± 2.3	-30.5 ± 3.3	23	16
21	PN M 1-2	133.12	-8.63	-28.4 ± 8.5	-12.1 ± 2	13	11
22	WeBo 1	135.67	1	-25.4 ± 4.6		33	17
23	NGC 1514	165.53	-15.29	42.3 ± 1.3	59.8 ± 4.4	21	10
24	H 3-75	193.65	-9.58	11.6 ± 2.6	22.9 ± 2	26	11
25	NGC 2346	215.7	3.62	31.5 ± 3.0	21.8 ± 0.9	13	10
26	PHR j0701-0749	221	-1.41	44.9 ± 2.9		14	11
27	LoTr 1	228.21	-22.14	15.8 ± 19.5:		31	19
28	PN V-V 1-7	235.44	1.89	38.9 ± 0.7		27	17
29	WRAY 15-158	255.33	-3.64	24.4 ± 2.3		22	19
30	LoTr 3	265.11	-4.21	16.2 ± 5.5	49 ± 3	19	15
31	NGC 3132	272.11	12.4	-11.1 ± 1.6	-16 ± 4.1	18	13
32	Hen 2-36	279.61	-3.19	-0.1 ± 1.5:	-7.1 ± 2	18	10
33	Hen 2-51	288.88	-5.22	13.5 ± 3.9	8 ± 3	13	12
34	Al 1	291.1	-39.66	1.1 ± 2.3:		16	15
35	Hen 2-70	293.61	1.2	64.6 ± 4.8		14	13
36	PN A66 35	303.57	40	-38.1 ± 4.6	-6.6 ± 3.8	9	8
37	SuWt 2	311.05	2.48	-15.7 ± 7.5	-40 ± 9	17	11
38	MPA J1508-6455	316.77	-5.8	-39.2 ± 11.9		43	17
39	Hen 2-134	319.22	-9.35	9.0 ± 0.7		45	21
40	PM 1-89	324.09	3.53	-68.5 ± 3.0	-81 ± 20	13	12
41	Hen 3-1312 (Sast 2-12)	334.84	-7.46	-70.6 ± 1.0	-77 ± -7	25	13
42	LoTr 5	339.89	88.46	-8.3 ± 1.7		21	13
43	Vd 1-1	344.27	4.75	-70.6 ± 1.0	-142.1 ± 2.5	11	10
44	SB 38	352.8	-8.41	-35.0 ± 7.0	59 ± 15	9	6
45	PHR J1711-3210	353.28	4.25	27.2 ± 1.7		10	6
46	PN G354.8+01.6	354.89	1.63	13.6 ± 6.6		13	10
47	Pe 1-11	358.01	-5.16	-11.9 ± 0.2	-130.6 ± 14	12	5
48	M 3-8	358.24	4.29	101.7 ± 3.4	95 ± 11	7	4
49	PHR J1752-3116	358.77	-2.5	-21.7 ± 8.4		2	1
50	Hen 3-1863	359.28	-33.5	4.3 ± 10.2:		19	14
51	Th 3-14	359.3	4.76	26.2 ± 20.4:	-239.2 ± 14	7	5